Available online at www.sciencedirect.com
ScienceDirect
Polyhedron 26 (2007) 2949–2956
POLYHEDRON
www.elsevier.com/locate/poly

Synthesis, structure and physical properties of trinuclear $M_3tdt_3(PEt_3)_3$ ($M = Fe^{II}$, Co^{II}) clusters containing metal–metal bonds

Mihyang Kim, Jaehong Han *

Metalloenzyme Research Group, BET Research Institute and Department of Biotechnology, Chung-Ang University, Anseong 456-756, Republic of Korea

Received 15 January 2007; accepted 29 January 2007
Available online 11 February 2007

Abstract

Trinuclear $M_3tdt_3(PEt_3)_3$ ($M = Fe^{II}$ for **I**, Co^{II} for **II**) clusters have been synthesized from the reaction between $M(PEt_3)_2Cl_2$ and Na_2tdt (tdt = toluene-3,4-dithiolate) in MeCN. Both complexes have been characterized by elemental analyses, FT-IR, UV–Vis, FAB-MS, ^1H NMR and cyclic voltammetry. Structures of $Fe_3tdt_3(PEt_3)_3$ (**I**) and $Co_3tdt_3(PEt_3)_3$ (**II**) were determined by single crystal X-ray crystallography. The Fe_3 triangular core of the 48-electron complex **I**, with an isosceles triangular geometry, showed very short Fe–Fe distances of 2.4014(13) and 2.4750(12) Å, which are comparable to the extensive M–M frameworks found in the FeMo-cofactor in nitrogenase. The isostructural $Co_3tdt_3(PEt_3)_3$ (**II**), with an analogous Co_3 coordination geometry, showed short Co–Co distances of 2.4442(9) and 2.5551(10) Å. The slightly longer M–M distances in complex **II** were explained by a total valence electron counting argument. Cyclic voltammetry of $Fe_3tdt_3(PEt_3)_3$ (**I**) showed robust reduction waves compared to $Co_3tdt_3(PEt_3)_3$ (**II**). Temperature-dependent effective magnetic moment measurements of **I** and **II** showed both clusters behave similarly and the magnetic property of the M_3 equilateral triangle core with extensive metal–metal interactions was characterized as degenerate frustration.

Keywords: Nitrogenase; Synthesis; Structure; Magnetic property; Metal–metal bonds; FeMo-cofactor

1. Introduction

The FeMo-cofactor in the MoFe protein of nitrogenase is a key complex for biological N_2 reduction [1]. The chemical formula of (*R*-homocitrate)$MoFe_7S_9X$ (X = unknown element) is unprecedented in biological or synthetic systems (Fig. 1). The identity of the unknown μ_6-atom was suggested as C, N or O by protein X-ray crystallography [2]. Although a nitrogen atom was favored by theoretical calculations [3], ENDOR and ESEEM spectroscopic studies did not find any evidences of a nitrogen atom [4]. One of the structural characteristics of the FeMo-cofactor is an extensive metal–metal (M–M) bonded framework. The Mo–Fe distances are found to be between 2.67 and 2.73 Å [2]. Especially, the trigonal prism of six Fe atoms shows very short Fe–Fe distances in a range between 2.58 and 2.67 Å. By comparison, most Fe/S clusters show Fe–Fe distances longer than 2.75 Å. The Fe–Fe bond lengths in the H-cluster of all-Fe hydrogenases are found between 2.57 and 2.62 Å, probably due to the π-acceptor CO and CN^- ligands [5–8]. The short M–M bonds in the FeMo-cofactor are unusual among biological inorganic clusters and the possible biological function of the M–M bonds in nitrogenase has been discussed [9]. Although it is controversial, synthetic Mo/Fe/S or Fe/S clusters with short M–M bonds may be of interest in understanding the mechanism of N_2 fixation in nitrogenase.

A plethora of metal-chalcogenide organometallic clusters have been reported, but inorganic clusters with a short Fe–Fe distance are rare. Recently, reactions under reducing conditions have been reported to produce $(Cl_4\text{-cat})_2Mo_2Fe_6S_8(PR_3)_6$ (R = Et, ^{n}Pr and ^{n}Bu) [10] and $(Cl_4\text{- cat})_2Mo_2Fe_3S_5(PEt_3)_5$ [11] compounds with short Mo–Fe and Fe–Fe bonds. These compounds were reported to show interesting chemical reactivity and physical properties.

* Corresponding author. Tel.: +82 31 670 4830.
E-mail address: jaehongh@cau.ac.kr (J. Han).

0277-5387/$ - see front matter © 2007 Elsevier Ltd. All rights reserved.
doi:10.1016/j.poly.2007.01.052

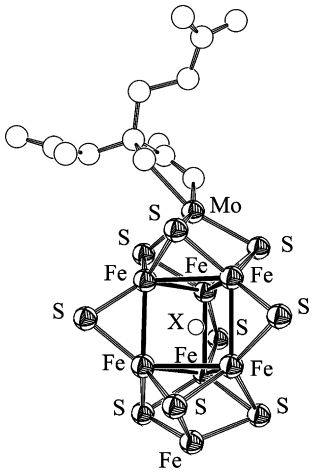

Fig. 1. Structure of FeMo-cofactor. The unknown atom is shown within the Fe_6 prismane frame (shown in solid bonds). The picture was generated by ORTEP-3 for Windows [35] after processing PDB data (1M1N) using Swiss-PdbViewer [36].

To understand the physical properties of clusters with short M–M bonds, we have prepared $M_3tdt_3(PEt_3)_3$ (**I** for M = Fe, **II** for M = Co) complexes from the reaction between $M(PEt_3)_2Cl_2$ and the bidentate thiolate ligand, Na_2tdt (where tdt = toluene-3,4-dithiolate). Although closely related complexes of $M_3tdt_3(P^nBu_3)_3$ (M = Fe or Co) and $Fe_3bdt_3(PEt_3)_3$ have been synthesized [13,14],[1] the synthetic method adopted here is different. Besides, due to the instability of the P^nBu_3 derivatives, these trinuclear Fe and Co clusters have never been completely characterized. The $M_3tdt_3(PEt_3)_3$ (**I** for M = Fe, **II** for M = Co) complexes were characterized structurally and physically by various methods. Complexes **I** and **II** are isostructural but have a different number of total valence electrons, so that shows different formal bond orders of the M–M bonds. These trinuclear $M_3tdt_3(PEt_3)_3$ complexes also are found to show interesting temperature-dependent magnetic properties.

2. Experimental

2.1. General

All experiments and reactions were carried out under a dinitrogen atmosphere using standard Schlenk line techniques or in an inert atmosphere glove box. All solvents were distilled under dinitrogen and nitrogen gas was bubbled through the solvents before each use in a glove box. $FeCl_2$, PEt_3 and toluene-3,4-dithiol were purchased from Aldrich and were used without further purification. Na_2tdt was prepared from the reaction between Na and toluene-3,4-dithiol in MeOH. The 2:1 molar ratio reaction resulted in a quantitative yield. $Fe(PEt_3)_2Cl_2$ was prepared from a 1:2 molar ratio of $FeCl_2$ and PEt_3 in THF. Anhydrous $CoCl_2$ was prepared by drying the hydrate form of $CoCl_2$ in a vacuum oven. A MeCN solution of $Co(PEt_3)_2Cl_2$ was prepared *in situ* from a 1:2 ratio of $CoCl_2$ and PEt_3.

^1H NMR spectra were recorded in $CDCl_3$ with a Bruker 400 MHz NMR spectrometer using non-deuteriated solvent as the internal standard. FT-IR spectra were collected on a Nicolet DX V. 4.56 FT-IR spectrometer in KBr pellets and the spectra were corrected for background effects. UV–Vis spectra were obtained on a Shimadzu UV-1601 UV–VIS spectrometer in the range 200–1000 nm. Elemental analyses were performed in the Microanalytical Laboratory at the University of Michigan. The data were corrected using acetanilide as a standard. FAB-Mass spectra were obtained with a 3-nitrobenzoyl alcohol matrix. Cyclic voltammetry was performed on a BAS-voltammograph. Three electrodes consisting of a glassy carbon working electrode, Pt auxiliary electrodes and a saturated calomel electrode (SCE) as a reference electrode were used for the measurements. $Fe_3tdt_3(PEt_3)_3$ (**I**) and $Co_3tdt_3(PEt_3)_3$ (**II**) were dissolved in 1,2-dichloroethane together with 0.1 M tetrabutylammonium hexafluorophosphate as a supporting electrolyte, and the scanning rate was 100 mV/s. Under the same conditions, 0.1 M of ferrocene in MeCN showed an oxidation wave at 480 mV. Magnetic susceptibilities of $Fe_3tdt_3(PEt_3)_3$ (**I**) and $Co_3tdt_3(PEt_3)_3$ (**II**) were measured in the temperature range of 4–300 K with a Quantum Design MPMS SQUID. The magnetic field of the measurements was 5000 G for the temperature-dependent experiments. The crystalline sample was put into a cellophane capsule under a dinitrogen atmosphere. The magnetic susceptibility of the holder was determined separately and diamagnetic corrections were estimated from Pascal's constants [15]. Magnetic moments per trinuclear cluster of **I** and **II** were reported.

2.2. $Fe_3tdt_3(PEt_3)_3$ (*I*)

$Fe(PEt_3)_2Cl_2$ (726 mg, 2.0 mmol) was dissolved in MeCN (30 mL) and Na_2tdt (400 mg, 2.0 mmol) was added into the solution. The reaction mixture turned immediately dark black and was stirred for 2 h, whereupon it turned reddish black. After overnight reaction, a reddish black precipitate was isolated by filtration. The product was extracted with diethyl ether (10 mL × 4) and the extract was dried under N_2. The black crystalline product was isolated in a 76.5% yield (500 mg, 0.51 mmol). ^1H NMR (CD_2Cl_2): $\delta = 32.5$ (br s, 9H, PCH_2CH_3), 14.6 (br s, 6H, PCH_2), 9.2 (br s), 8.2 (br d), 6.4 (br d), 1.6 (br d), 0.6 (br s), 0.08 (br s, 3H, tdt-CH_3), −0.1 (br s), −0.64 (br s), −11.2 (br s, 12H, PCH_2), −14.5 (br t, 18H, PCH_2CH_3). ($CDCl_3$): $\delta = 44.3$ (br s), 43.4 (br s), 14.75 (br s, 12H, PCH_2), 11.0 (t, 9H, PCH_2CH_3), 6.9 (br s), 6.6 (br s), 5.16 (br s, 9H, PCH_2CH_3), 2.24 (br s), 1.98 (br s), 0.58 (br s), 0.05 (br s, 9H, tdt-CH_3), −2.46 (br s, 9H, PCH_2CH_3), −4.94 (br s, 6H, PCH_2), −17 (br s), −43 (br s). FT-IR (KBr, cm^{-1}, relative intensity) 3032(m), 2956(m), 2929(s), 2897(m), 2873(s), 1450(s), 1031(vs) 761(s). Far-IR (KBr, cm^{-1}, relative intensity) 408(s), 356(s), 333(s). FAB^+-MS

[1] bdt = 1,2-benzenedithiolate.

(NBA, *m/z*) 984.1 ($[Fe_3tdt_3(PEt_3)_3]^+$), 868.1 ($[Fe_3tdt_3(PEt_3)_2]^+$), 748.0 ($[Fe_3tdt_3(PEt_3)]^+$), 629.9 ($[Fe_3tdt_3]^+$). *Anal.* Calc. for $C_{41}H_{68}Fe_3O_{0.5}P_3S_6$ (**I**, MW1021.83): C, 48.19; H, 6.71. Found: C, 47.48; H, 6.75%. UV–Vis (nm ($M^{-1}\,cm^{-1}$), purple in Et_2O): λ_{max} (ε) = 258 (7900), 275 (sh, 6200), 326 (sh, 2900), 650 (750). Cyclic voltammetry[2] (1,2-dichloroethane, 0.1 M of Et_4NPF_6) 0.74 (irr), 0.42 (irr), 0.08 (irr), −0.30 (rev), −0.52 (rev), −0.76 (rev).

2.3. $Co_3tdt_3(PEt_3)_3$ (**II**)

Anhydrous $CoCl_2$ (650 mg, 5.0 mmol) was dissolved in 15 mL of MeCN and stirred for 30 min to dissolve the $CoCl_2$. To this sky blue solution, PEt_3 (1.5 mL, 10.0 mmol) was added and the color of the solution changed to dark blue. The reaction mixture was filtered through a glass filter after 5 min. To the *in situ* prepared $Co(PEt_3)_2Cl_2$ MeCN solution was added Na_2tdt (1.0 g, 5 mmol) and the reaction mixture changed color immediately to yellowish black. After about 2 h, the reaction mixture turned greenish black. After stirring overnight, the reaction was stopped by filtration and a black precipitate was isolated. The precipitate was extracted with diethyl ether (20 mL × 4). The diethyl ether solvent was removed under N_2 and a golden black crystalline product was isolated in a 72.6% yield (1.2 g, 1.21 mmol). ^1H NMR (CD_2Cl_2): δ = 92.2 (br s), 8.0 (br s), 6.9 (br s), 6.6 (br s), 6.4 (br s), 4.1 (br s), 3.75 (br s), 3.44 (br s, 6H, PCH_2), 2.1(m), 1.83(m), 1.64(m), 1.27 (br s), 1.11 (t, 18H, PCH_2CH_3), 0.053 (br s, 9H, tdt-CH_3), −0.37 (br s, 9H, PCH_2CH_3), −1.16 (br s, 6H, PCH_2), −1.84 (br s, 6H, PCH_2), −2.44 (br s). FT-IR (KBr, cm^{-1}, relative intensity) 3030(m), ν(C–H of PEt_3); 2956(m), 2929(s), 2899(m), 2874(s), 1447(s), 1030(vs) 762(s). Far-IR (KBr, cm^{-1}, relative intensity) 414(s), 345(s), 333(s). FAB^+-MS (NBA, *m/z*) 993.2 ($[Co_3tdt_3(PEt_3)_3]^+$), 875.1 ($[Co_3tdt_3(PEt_3)_2]^+$), 756.9 ($[Co_3tdt_3(PEt_3)]^+$), 638.8 ($[Co_3tdt_3]^+$). *Anal.* Calc. for $C_{41}H_{68}Co_3O_{0.5}P_3S_6$ (**II**, MW 1031.10): C, 47.76; H, 6.65. Found: C, 47.34; H, 6.42%. UV–Vis (nm ($M^{-1}\,cm^{-1}$), green in Et_2O): λ_{max} (ε) = 263 (6000), 275 (sh, 5200), 328 (sh, 2400), 391 (2060). Cyclic voltammetry (1,2-dichloroethane, 0.1 M of Et_4NPF_6) 0.72 (irr), 0.5 (irr), −0.37 (rev), −0.51 (rev).

2.4. X-ray crystallography

Black rhombic-shaped crystals of $Fe_3tdt_3(PEt_3)_3$ (**I**) and $Co_3tdt_3(PEt_3)_3$ (**II**) were obtained from the ether extract of the reaction precipitate. The diffraction data were collected at 158(2) and 123(2) K for **I** and **II**, respectively, using a Bruker SMART area diffractometer. The crystal data and structural parameters are shown in Tables 1 and 2. The structures for compounds **I** and **II** were solved by direct methods to locate heavy atoms, and the non-hydrogen atoms were located through subsequent difference Fourier syntheses. Structural refinement was carried out by full-matrix least squares on F^2. All non-hydrogen atoms were refined with anisotropic thermal parameters. Hydrogen atoms were placed in calculated positions, allowed to ride on their corresponding atoms and refined isotropically except those on disordered carbon atoms. The carbon atoms of diethyl ether solvent molecules in **I** and **II** were severely disordered and the geometry restraints did not improve the refinement. All calculations were performed using SHELXTL-NT V. 5.1 software.

Table 1
Crystal data and structure refinement for $Fe_3tdt_3(PEt_3)_3$ (**I**) and $Co_3tdt_3(PEt_3)_3$ (**II**)

	$Fe_3tdt_3(PEt_3)_3$ (**I**)	$Co_3tdt_3(PEt_3)_3$ (**II**)
Empirical formula	$C_{82}H_{136}Fe_6OP_6S_{12}$	$C_{82}H_{136}Co_6OP_6S_{12}$
Formula weight	2043.55	2062.03
Temperature (K)	158(2)	123(2)
Wavelength (Å)	0.71073	0.71073
Crystal system	triclinic	triclinic
Space group	$P\bar{1}$	$P\bar{1}$
Unit cell dimensions		
a (Å)	11.3437(13)	11.301(4)
b (Å)	12.8765(15)	12.812(4)
c (Å)	33.108(4)	32.950(10)
α (°)	83.171(2)	83.326(5)
β (°)	85.415(2)	85.110(5)
γ (°)	89.195(2)	89.081(5)
Volume (Å^3)	4786.3(9)	4721.3(3)
Z	2	2
D_{calc} (Mg/m^3)	1.418	1.450
Absorption coefficient (mm^{-1})	1.289	1.439
F(000)	2148	2160
Crystal size (mm^3)	0.24 × 0.12 × 0.1	0.36 × 0.12 × 0.09
Θ Range for data collection (°)	1.59–24.76	1.78–26.51
Index ranges	$-13 \leqslant h \leqslant 13$, $-15 \leqslant k \leqslant 15$, $-38 \leqslant l \leqslant 39$	$-14 \leqslant h \leqslant 14$, $-16 \leqslant k \leqslant 16$, $-41 \leqslant l \leqslant 41$
Reflections collected	39215	86387
Independent reflections	16283	19418
R_{int}	0.0696	0.0821
Completeness to theta	24.76°, 99.2%	26.51°, 99.1%
Refinement method	full-matrix least-squares	full-matrix least-squares
Data/restraints/parameters	on F^2	on F^2
Goodness-of-fit on F^2	16283/0/964	19418/0/964
Final *R* indices [$I > 2\sigma(I)$]	0.899	1.018
R indices (all data)	$R_1 = 0.0561$, $wR_2 = 0.1194$	$R_1 = 0.0484$, $wR_2 = 0.0980$
	$R_1 = 0.1226$, $wR_2 = 0.1327$	$R_1 = 0.1000$, $wR_2 = 0.1142$

3. Results and discussion

3.1. Synthesis

Many Mo/Fe/S clusters as a model system of the FeMo-cofactor in the nitrogenase MoFe protein have been

[2] The redox potentials were reported versus SCE. rev = reversible, qr = quasi-reversible.

Table 2
Selected bond lengths (Å) and angles (°) for $Fe_3tdt_3(PEt_3)_3$ (**I**) and $Co_3tdt_3(PEt_3)_3$ (**II**)

$Fe_3tdt_3(PEt_3)_3$ (**I**)		$Co_3tdt_3(PEt_3)_3$ (**II**)	
Fe(1)–Fe(2)	2.4635(12)	Co(1)–Co(2)	2.5353(10)
Fe(1)–Fe(3)	2.4750(12)	Co(1)–Co(3)	2.5421(10)
Fe(2)–Fe(3)	2.4016(13)	Co(2)–Co(3)	2.4442(9)
Fe(4)–Fe(5)	2.4747(13)	Co(4)–Co(5)	2.5551(10)
Fe(4)–Fe(6)	2.4737(12)	Co(4)–Co(6)	2.5308(10)
Fe(5)–Fe(6)	2.4014(13)	Co(5)–Co(6)	2.4470(11)
Fe(1)–S(1)	2.2247(18)	Co(1)–S(1)	2.2250(14)
Fe(1)–S(2)	2.2226(19)	Co(1)–S(2)	2.2172(13)
Fe(1)–S(3)	2.2320(19)	Co(1)–S(3)	2.2170(14)
Fe(1)–S(4)	2.2271(18)	Co(1)–S(4)	2.2190(14)
Fe(2)–S(1)	2.2936(17)	Co(2)–S(1)	2.3047(13)
Fe(2)–S(3)	2.2896(18)	Co(2)–S(3)	2.3049(13)
Fe(2)–S(5)	2.2795(19)	Co(2)–S(5)	2.2872(14)
Fe(2)–S(6)	2.2641(18)	Co(2)–S(6)	2.2630(13)
Fe(3)–S(2)	2.2955(17)	Co(3)–S(2)	2.3081(13)
Fe(3)–S(4)	2.2947(18)	Co(3)–S(4)	2.3113(14)
Fe(3)–S(5)	2.2658(18)	Co(3)–S(5)	2.2696(14)
Fe(3)–S(6)	2.2809(18)	Co(3)–S(6)	2.2870(14)
Fe(4)–S(7)	2.225(2)	Co(4)–S(7)	2.2160(15)
Fe(4)–S(8)	2.2268(18)	Co(4)–S(8)	2.2165(14)
Fe(4)–S(9)	2.2251(17)	Co(4)–S(9)	2.2168(14)
Fe(4)–S(10)	2.223(2)	Co(4)–S(10)	2.2201(14)
Fe(5)–S(7)	2.2910(18)	Co(5)–S(7)	2.2983(15)
Fe(5)–S(9)	2.2862(18)	Co(5)–S(9)	2.2932(13)
Fe(5)–S(11)	2.2591(19)	Co(5)–S(11)	2.2499(14)
Fe(5)–S(12)	2.267(2)	Co(5)–S(12)	2.2676(14)
Fe(6)–S(8)	2.2987(18)	Co(6)–S(8)	2.3091(15)
Fe(6)–S(10)	2.306(2)	Co(6)–S(10)	2.3295(15)
Fe(6)–S(11)	2.302(2)	Co(6)–S(11)	2.3100(16)
Fe(6)–S(12)	2.2894(19)	Co(6)–S(12)	2.2942(14)
Fe(1)–P(1)	2.2752(18)	Co(1)–P(1)	2.1891(13)
Fe(2)–P(2)	2.265(2)	Co(2)–P(2)	2.1857(13)
Fe(3)–P(3)	2.268(2)	Co(3)–P(3)	2.1873(14)
Fe(4)–P(4)	2.2744(19)	Co(4)–P(4)	2.1920(14)
Fe(5)–P(5)	2.269(2)	Co(5)–P(5)	2.1877(15)
Fe(6)–P(6)	2.283(2)	Co(6)–P(6)	2.1931(14)
Fe(2)–Fe(1)–Fe(3)	58.20(3)	Co(2)–Co(1)–Co(3)	57.55(2)
Fe(1)–Fe(2)–Fe(3)	61.14(4)	Co(1)–Co(2)–Co(3)	61.36(2)
Fe(2)–Fe(3)–Fe(1)	60.66(4)	Co(2)–Co(3)–Co(1)	61.09(3)
Fe(5)–Fe(4)–Fe(6)	58.06(4)	Co(5)–Co(4)–Co(6)	57.52(3)
Fe(4)–Fe(5)–Fe(6)	60.95(4)	Co(4)–Co(5)–Co(6)	60.74(3)
Fe(4)–Fe(6)–Fe(5)	60.99(4)	Co(4)–Co(6)–Co(5)	61.74(2)
S(1)–Fe(1)–S(4)	156.64(7)	S(1)–Co(1)–S(4)	154.51(5)
S(2)–Fe(1)–S(3)	155.97(7)	S(2)–Co(1)–S(3)	154.98(5)
S(5)–Fe(2)–S(3)	156.11(7)	S(5)–Co(2)–S(1)	154.58(5)
S(6)–Fe(2)–S(1)	157.13(7)	S(6)–Co(2)–S(3)	155.80(5)
S(5)–Fe(3)–S(4)	156.39(7)	S(5)–Co(3)–S(2)	155.02(5)
S(6)–Fe(3)–S(2)	155.81(7)	S(6)–Co(3)–S(4)	154.51(5)
S(7)–Fe(4)–S(10)	156.18(8)	S(7)–Co(4)–S(10)	154.78(5)
S(8)–Fe(4)–S(9)	156.07(7)	S(8)–Co(4)–S(9)	154.41(5)
S(11)–Fe(5)–S(9)	157.16(8)	S(11)–Co(5)–S(9)	155.38(5)
S(12)–Fe(5)–S(7)	156.73(8)	S(12)–Co(5)–S(7)	154.84(5)
S(12)–Fe(6)–S(8)	156.25(7)	S(12)–Co(6)–S(8)	155.23(5)
S(11)–Fe(6)–S(10)	155.44(8)	S(11)–Co(6)–S(10)	154.14(5)

synthesized. These complexes were mainly achieved through self-assembly, exploiting the thermodynamic stability of the products [16,17], or rational assembly of simple building blocks under reducing conditions [11,18–20]. The complexes from the reducing conditions usually possess a reduced core with short M–M bonds. Although trigonal M_3 (M = Fe, Co) complexes with bidentate thiolate bridging ligands and trialkylphosphine terminal ligands have been reported [12–14], the synthesis of $M_3tdt_3(PEt_3)_3$ (M = Fe, Co) has never been published. The complex $Fe_3tdt_3(P^nBu_3)_3$ prepared from EtOH was reported to be unstable, but its PEt_3 analog, **I**, was stable enough for various physical characterizations. Although it was suggested that the electron-donating methyl group on the phenyl ring would destabilize the complex [14], the effect of methyl substitution seems to be negligible because it stays too remote from the metal ions. Rather, the relative electron-donating property of P^nBu_3 would be a more significant contributor to the stability of the complex [21]. Since PEt_3 is a comparatively stronger electron-withdrawing ligand than P^nBu_3, when we introduced PEt_3 to stabilize the M_3 core, the product $Fe_3tdt_3(PEt_3)_3$ (**I**) could be isolated even at room temperature. The Co analog, $Co_3tdt_3(PEt_3)_3$ (**II**), was also successfully prepared using anhydrous $CoCl_2$ under the same reaction conditions. The product **II** from the reaction was very soluble in MeCN. Diethyl ether extraction of the reaction precipitate was an efficient method to purify complex **II**. It should be pointed out that a minimum amount of MeCN is necessary to produce enough precipitate for the isolation of **II**. Both products were very soluble in most organic solvents.

The reaction conditions of using a 1:2 ratio of $FeCl_2$ and PEt_3 is reminiscent of $Fe(PEt_3)_2Cl_2$ in Mo/Fe/S and Fe/S chemistry. The reaction of $[(Cl_4\text{-cat})Mo(MeCN)Fe_3S_4Cl_3]^{2-}$ with $Fe(PEt_3)_2Cl_2$ produces the $(Cl_4\text{-cat})_2Mo_2Fe_6S_8(PEt_3)_6$ cluster and the reaction between $[Fe_4S_4Cl_4]^{2-}$ and $Fe(PEt_3)_2Cl_2$ produces the $Fe_6S_6(PEt_3)_4Cl_2$ cluster [11].

3.2. Structure

The single crystal X-ray structures of $Fe_3tdt_3(PEt_3)_3$ (**I**) and $Co_3tdt_3(PEt_3)_3$ (**II**) are shown in Figs. 2 and 3, respectively. The crystal data and structure refinement details, and selected bond lengths (Å) and angles (°) for complexes **I** and **II** are shown in Tables 1 and 2, respectively. Both structures are isostructural and crystallized in the same unit cell system with the same space group. Even the diethyl ether solvent molecules are found in the same positions for both X-ray structures.

Due to the asymmetric methyl position of the bridging tdt ligands, two different structural isomers of **I** were found in the triclinic unit cell (Fig. 2). The first molecule (**IA**) has a *cis*-arrangement of two methyl groups of tdt ligands on the Fe(1) center, while the second molecule (**IB**) shows a *trans*-arrangement of tdt ligands around the Fe(4) center. The same type of isomerism is found in the solid structure of $Co_3tdt_3(PEt_3)_3$ (**II**). The structure of the $Fe_3tdt_3(PEt_3)_3$ (**I**) cluster can be described as an isosceles triangle Fe_3 metal cluster with two long Fe–Fe bonds and one short Fe–Fe bond. The formation of the Fe_3 isosceles triangle geometry, instead of an equilateral triangle geometry, can be explained by different bridging modes of the tdt ligands (see Fig. 3). The Fe centers in **I** show coordination geome-

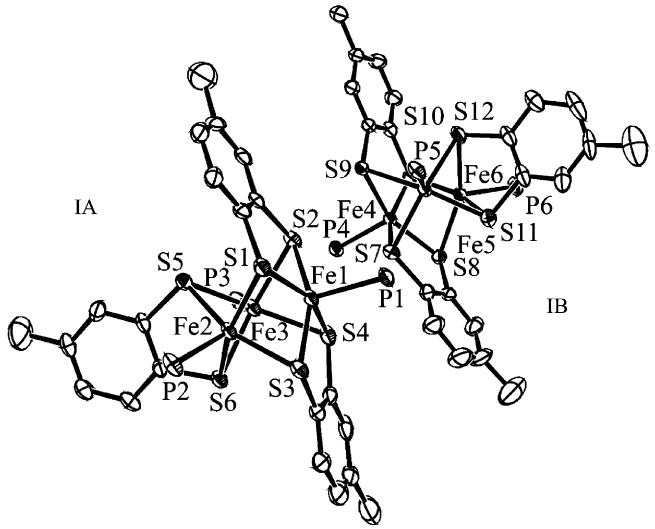

Fig. 2. Single-crystal X-ray structure of $Fe_3tdt_3(PEt_3)_3$ (**I**). Fe–Fe bonds, hydrogen atoms and ethyl groups of PEt_3 were omitted for clarity. Two unique molecules generated by different positions of the toluene methyl groups are shown.

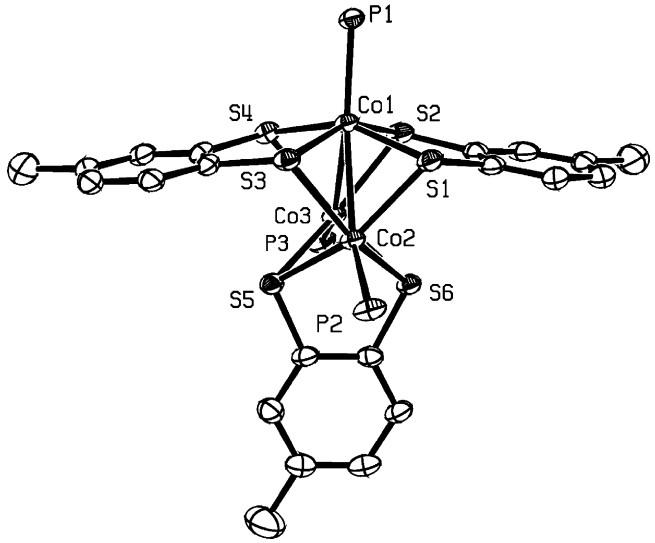

Fig. 3. Single-crystal X-ray structure of $Co_3tdt_3(PEt_3)_3$ (**II**). Hydrogen atoms and ethyl groups of PEt_3 were omitted for clarity.

tries of distorted square pyramids with a phosphorus axial ligand and four sulfur equatorial ligands. The toluene-3, 4-dithiolate ligand, with two bridging thiolates, is a eight-electron donor and the triethylphosphine terminal ligand is a two-electron donor [22]. The total number of valence electrons of 48 in **I** is six electrons fewer than the number expected for three-metal clusters based on the Wade–Mingos–Lauher rule [23]. Therefore, the Fe–Fe bonds in the $Fe_3tdt_3(PEt_3)_3$ (**I**) cluster are expected to have three formal metal–metal single bonds. Likewise, the total number of valence electrons in **II** is 51 and the complex is expected to have three Co–Co bonds with a formal bond order of 0.5. Such formal M–M bond order arguments can explain the differences of the bond distances between **I** and **II**.

The short Fe–Fe bond distances in **I** are 2.4016(13) and 2.4014(13) Å, which is longer than the value of 2.380(2) Å found for the $Fe_3tdt_3(P^nBu)_3$ complex [14]. The other long Fe–Fe distances are found to be in the range 2.4635(12)–2.4750(12) Å, and those of $Fe_3tdt_3(P^nBu)_3$ are 2.493(2) and 2.499(2) Å. The Fe–Fe bonds in the $Fe_3tdt_3(PEt_3)_3$ (**I**) cluster are even shorter than those found in the FeMo-cofactor of nitrogenase. Fe–Fe bonds distances in the FeMo-cofactor are found in the range between 2.58 and 2.67 Å. Two different ranges of Fe–S distances are found in complex **I**. The dithiolate ligands on the Fe(1) and Fe(4) centers have short Fe–S distances with an average value of 2.2258(10) Å.[3] The thiolate ligands on the other Fe centers show an average Fe–S distance of 2.285(4) Å. The difference of 0.06 Å is significant and implies a multiple Fe–S bond order between Fe(1)/Fe(4) and thiolate S [24]. Therefore, all three Fe–Fe bonds in the $Fe_3tdt_3(PEt_3)_3$ (**I**) cluster do not seem to have equally single-bond character and, instead, some Fe–S bonds also have multiple bond character. It could be another reason why the Fe_3 core has an isosceles triangular geometry.

Two unique molecules of the $Co_3tdt_3(PEt_3)_3$ (**II**) cluster in the unit cell do not exhibit significant differences from those of **I** and isosceles triangles of three cobalt ions are found. The Co_3 geometry is slightly different from the Fe_3 geometry, and the average vertex angle of the Co_3 and Fe_3 cores are found to be 57.54(3)° and 58.13(7)°, respectively. The Co–Co distances of **II** are significantly different, and are compared to **I** in Table 2. While the Fe–Fe distances of the legs of the isosceles Fe_3 core in **I** are in the range 2.4635(12)–2.4750(12) Å, the corresponding Co–Co distances of the isosceles Co_3 core in **II** are in the range 2.5308(10)–2.5551(10) Å. The base of the isosceles Co_3 core in **II** has an average Co–Co distance of 2.4456(14) Å , which is much longer than 2.4015(13) Å, the average distance of the isosceles base of the Fe_3 core in **I**. The average distance of the long Co–Co bonds is 2.541(5) Å and the average distance of the long Fe–Fe bonds is 2.472(3) Å. Average M–M distances of $Fe_3tdt_3(PEt_3)_3$ (**I**) and $Co_3tdt_3(PEt_3)_3$ (**II**) are 2.472(3) and 2.541(5) Å, respectively. Like complex **I**, two types of Co–S bonds are found in **II**. Co–S bonds around Co(1) and Co(4) atoms have an average distance of 2.2185(14) Å, which is shorter than the average distance of the other Co–S bonds (2.294(5) Å), and even shorter than the short Fe(1)/Fe(4)–S bond (average 2.2258(10) Å). It seems the Co(1)/Co(4)–S bonds of the $Co_3tdt_3(PEt_3)_3$ (**II**) cluster have more multiple bond character than **I** due to the non-integer bond order among the Co–Co bonds; three Co–Co bonds have a formal bond order of 0.5. It should be pointed out that each Co atom in

[3] The number in parenthesis represents the larger of the individual standard deviations or the standard deviation from the mean, $\sigma = [\sum_{i=1}^{n}(x_i - x)^2/n(n-1)]^{1/2}$, where x_i is an individual standard deviation, x is the average of individual standard deviations, and n is the number of individual standard deviations.

complex **II** has one more valence electron than each of the Fe atoms in complex **I**. Because both complexes are exactly same except for the metal ions, complex **II** may need less Co–Co bonding.

In organometallic clusters [25], the Fe–Fe distances of compounds with Fe–Fe double bonds are found in the range 2.215–2.326(4) Å. For the dinuclear organometallic clusters $Fe_2(NO)_2(\eta\text{-}C_5H_5)_2$ and $Co_2(NO)_2(\eta\text{-}C_5H_5)_2$, M–M distances of 2.326 and 2.372 Å are found for formal bond orders of 2 and 1.5, respectively [22,26]. The Fe_4S_4 cluster of the all-ferrous Fe protein, formally a 56-electron complex with two Fe–Fe double bonds and two Fe–Fe single bonds, shows two Fe–Fe distances at 2.52 Å and one Fe–Fe distance at 2.77 Å [27]. FeMo-cofactor with a $[Mo^{4+}4Fe^{2+}3Fe^{3+}(\mu\text{-}S)_3(\mu_3\text{-}S)_6(\mu_6\text{-}X)_6]$ core is supposed to have multiple M–S and M–M bonds and shows Fe–Fe distances between 2.58 and 2.67 Å [9,28]. The Fe–Fe bonds with distances of 2.4683(9) and 2.4721(9) Å found in $(Cl_4\text{-}cat)_2Mo_2Fe_3S_5(PEt_3)_5$ were suggested as intermediate of single and double bonds [11]. The average M–M distances of **I** and **II** are 2.448(15) and 2.509(20) Å, respectively. For comparison, the $Ni_3(S_2C_{10}Cl_6)_3(PPh_3)_3$ complex prepared from Ni(0) was reported to have a similar isosceles Ni_3 core as complexes of **I** and **II** do [29]. The Ni–Ni distance in this 54-electron complex was to be 2.641(4) Å.

3.3. Physical properties

^{1}H NMR spectra of $Fe_3tdt_3(PEt_3)_3$ (**I**) and $Co_3tdt_3(PEt_3)_3$ (**II**) in CD_2Cl_2 showed a broad distribution of the peaks. The chemical shifts of protons in complex **I** were found between 33 and −15 ppm, and those in complex **II** were found between 93 and −3 ppm. The wide range of chemical shifts can be attributed to paramagnetism and the high spin configuration of the complexes. Peaks from tdt were almost unassignable and only verified the asymmetric chemical environments of the protons. The dark red KBr pellet of **I** showed aromatic C–H stretching at 3032 cm^{-1} and the characteristic C–H stretching of PEt_3 at 2956, 2929, 2897 and 2873 cm^{-1}. The IR spectra of **I** and **II** are almost identical in both mid- and far-IR ranges. The chemical compositions of **I** and **II** were confirmed by CHN analysis and FAB^+-MS, and the isotope distributions of the molecular ion peaks of **I** and **II** were well matched to those of theoretical expectation.

UV–Vis spectra were measured in diethyl ether (Fig. 4). The purple solution of $Fe_3tdt_3(PEt_3)_3$ (**I**) showed absorptions at 258, 275, 326 and 650 nm and the green solution of $Co_3tdt_3(PEt_3)_3$ (**II**) showed similar absorptions at 263, 275, 328 and 391 nm. The absorption at 391 nm in **II** was found in place of the 650 nm absorption in **I**. Whilst the spectrum of **II** did not change, **I** in diethyl ether changed on exposure to air. The purple diethyl ether solution of **I** turned to dark blue upon air-oxidation and showed absorptions at 216, 252, 320, 370 and 522 nm (Fig. 5), which is reminiscent of the air-oxidation of the FeMo-cofactor. The dark green solution of the FeMo-cofactor was reported to show an absorption band at around 510 nm upon air-oxidation [30].

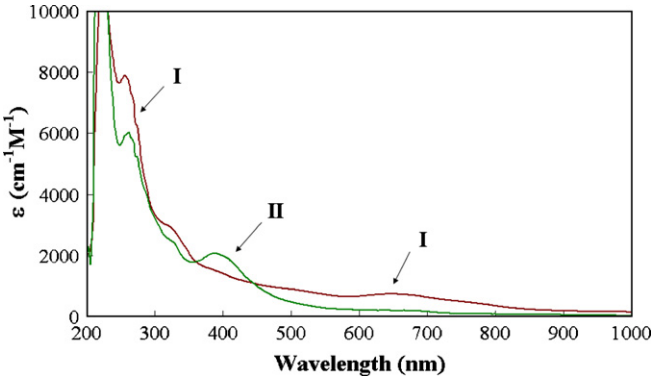

Fig. 4. UV–Vis spectra of $Fe_3tdt_3(PEt_3)_3$ (**I**) and $Co_3tdt_3(PEt_3)_3$ (**II**) in diethyl ether.

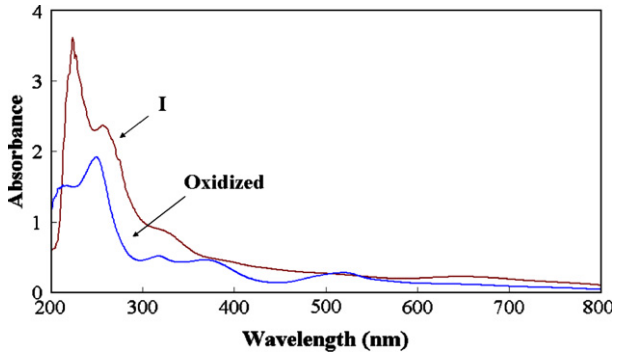

Fig. 5. UV–Vis spectrum change of $Fe_3tdt_3(PEt_3)_3$ (**I**) upon air-oxidation in diethyl ether.

3.4. Electrochemistry

The cyclic voltammetry of the complex $Fe_3tdt_3(PEt_3)_3$ (**I**) showed multiredox waves (Fig. 6). In CH_2ClCH_2Cl, **I** showed three reversible reduction waves at −0.30, −0.52 and −0.76 V and three irreversible oxidation waves at 0.74, 0.42 and 0.08 V. The three reversible reductions are very close, within a 460 mV potential spread, and corre-

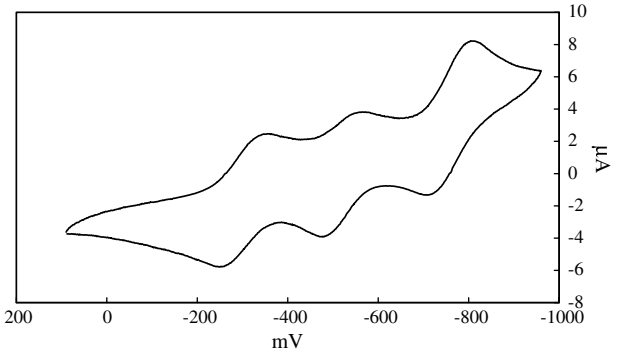

Fig. 6. Cyclic voltammetric responses of $Fe_3tdt_3(PEt_3)_3$ (**I**) in CH_2ClCH_2Cl.

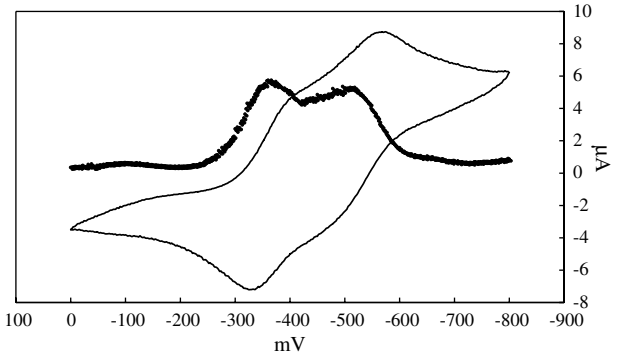

Fig. 7. Cyclic voltammetric responses of $Co_3tdt_3(PEt_3)_3$ (**II**) in CH_2ClCH_2Cl. The overlaid plot shows differential pulse voltammetry at the same potential.

spond to $\mathbf{I}^{0/-1}$, $\mathbf{I}^{-1/-2}$ and $\mathbf{I}^{-2/-3}$ reductions, respectively. Reduction of Fe(II) centers to Fe(I) ions is not physically feasible and only a two-electron reduction process is possible.[4] The observed three reversible reductions of **I** may be explained by the fact that the three M–M single bonds can accept multi-electrons. Such an exploitation of a M–M bond for electron transfer is very important for the catalytic mechanism of nitrogenase FeMo-cofactor and the direct possibility has been suggested before [9]. The complex $Co_3tdt_3(PEt_3)_3$ (**II**) showed a smaller number of redox waves than **I** (Fig. 7). The reduction waves of **II** are found at −0.37 and −0.51 V, and are only 0.14 V apart. Two independent reductions were confirmed by differential pulse voltammetry. Two irreversible oxidations at 0.72 and 0.5 V also were observed. Complex **I** showed much more versatile redox waves compared to complex **II**, which can be explained by the fact that $Fe_3tdt_3(PEt_3)_3$ (**I**) is more coordinatively unsaturated by total valence electron count arguments. It seems that the M–M bonds in the clusters are able to act as an electron reservoir and accept multi-electrons within a short range of potentials. This may be the reason why the FeMo-cofactor shows an extensive M–M bonding framework, so that multi-electron reduction of N_2 is possible.

3.5. Magnetic study

The magnetic susceptibilities of $Fe_3tdt_3(PEt_3)_3$ (**I**) and $Co_3tdt_3(PEt_3)_3$ (**II**) were measured over various temperatures at 5000 G, and field dependency experiments showed almost linear responses. $Fe_3tdt_3(PEt_3)_3$ (**I**) with three Fe(II) ions in an isosceles triangular geometry showed $\mu_{eff} = 2.60$ BM at 310 K, and the value is close to that for a $S_T = 1$ spin-state. The paramagnetic property of **I** is evident by ^{1}H NMR measurement at room temperature, which shows broad proton resonances between −43 and 45 ppm in $CDCl_3$. The mononuclear $Fe(bdt)_2(PMe_3)$ complex with a square pyramidal geometry was reported to show a low-spin/high-spin equilibrium [24]. Although it has a Fe(IV) center, this report suggests a possible spin-transition of the dithiolate phosphine Fe complex. The magnetic moment of **I** decreased to 0.31 μ_B when the temperature was lowered to 100 K (Fig. 8), which shows a strong antiferromagnetic coupling of the spin system. Below 100 K, the magnetic moment increases to 0.66 μ_B (15 K) and decreases again slightly to 0.60 μ_B (up to 4.2 K). The exchange coupling constants from the magnetic susceptibility data could not be obtained with the isotropic Heisenberg model [15].

Complex **II** showed temperature-dependent magnetic susceptibility similar to complex **I**, but with small exchange couplings (Fig. 8). This may be because complex **II** ia a three $S = 3/2$ system while complex **I** is a three $S = 2$ system. The magnetic moments of **I** and **II** at room temperature happen to be similar to each other. The magnetic moment of **II** (2.52 μ_B at 300 K) decreases to 1.76 μ_B at 80 K, probably due to the antiferromagnetic couplings. Below 80 K, the magnetic moment increases slowly to 1.84 μ_B (10 K) and decreases again slightly to 1.83 μ_B (up to 4 K). The complex $Co_3(bdt)_3(P^nBu_3)_3$ was reported to show an effective magnetic moment μ_{eff} of 2.6 μ_B at room temperature. Although it was suggested to have three low-spin Co^{II} (d^7, $S = 1/2$) atoms [14], our measurements, including ^{1}H NMR, suggest that complex **II** has three antiferromagnetically coupled high-spin Co^{II} centers. Similar temperature-dependent magnetic susceptibility was observed from the $(Cl_4\text{-cat})_2Mo_2Fe_3S_5(PEt_3)_5$ complex, which also has strong M–M interactions with a very short Fe–Fe distance. The complex has three Fe(II) centers with the same coordination environments as complexes **I** and **II**. The magnetic moment of the $(Cl_4\text{-cat})_2Mo_2Fe_3S_5(PEt_3)_5$ complex increased from 9.10 μ_B at 325 K to 10.96 μ_B at 95 K, and then decreased steeply to 3.08 μ_B at 4 K [11].

This type of temperature-dependent magnetic susceptibility change is unusual, and the observed spin-state

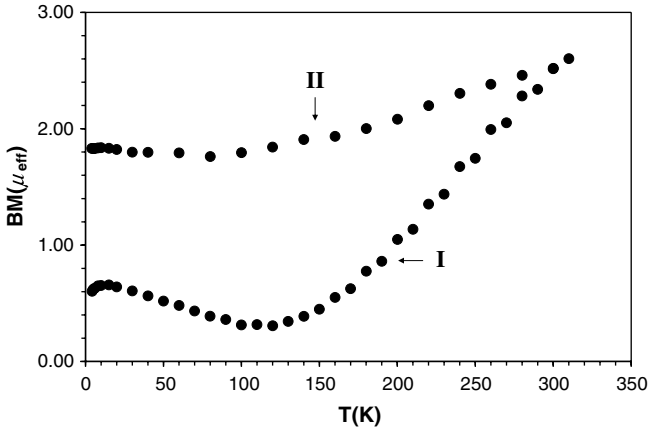

Fig. 8. Molar magnetic susceptibility of $Fe_3tdt_3(PEt_3)_3$ (**I**) and $Co_3tdt_3(PEt_3)_3$ (**II**), plotted μ_{eff} (per trinuclear cluster) versus temperature.

[4] Standard reduction potentials for Fe(III)/Fe(II) and Fe(II)/Fe(0) are 0.77 and −0.44 V, respectively.

transition has three possible explanations, namely spin crossover [31], spin-frustration [32] and degenerate frustration [33]. Thermal spin crossover for the magnetic properties of **I** and **II** can be excluded due to the complicated temperature-dependent magnetic susceptibility changes. Usual thermal spin crossover shows a directional magnetic moment change at a certain temperature. Spin-frustration is a status where geometric constraints of the molecule prevent neighboring spins from adopting a configuration of minimized magnetic energy [34]. But the strict meaning of spin-frustration is a state where the system cannot remain in a single ground state, which does not seem to be the case of the M_3 equilateral triangle complex [33]. Kahn also pointed out that this type of magnetic phenomena occurs whenever the symmetry of the system forces the magnetic ground state to be degenerate and not correspond to any defined spin coupling scheme. Therefore, the more precise terminology for the magnetism would be degenerate frustration. Although some of the clusters with short M–M distances, $(Cl_4\text{-cat})_2Mo_2Fe_3S_5(PEt_3)_5$ and complexes **I** and **II**, have shown the interesting magnetic property of degenerate frustration, there is no physical evidence that such a property is related to the metal–metal bonds.

In summary, we have successfully synthesized and characterized trinuclear $M_3tdt_3(PEt_3)_3$ ($M = Fe^{II}$, Co^{II}) clusters. These clusters show short M–M bonds and the M–M distance differences between **I** and **II** were explained by total valence electron counting arguments. Versatile redox behavior of the $M_3tdt_3(PEt_3)_3$ ($M = Fe^{II}$, Co^{II}) clusters is probably due to the valence unsaturation characteristics of the complexes, which may be relevant to the catalytic mechanism of nitrogenase FeMo-cofactor. The temperature-dependent magnetic susceptibility of these trinuclear clusters were also characterized as a degenerate frustration system, but the strong M–M interactions do not seem to be related to the unusual magnetic properties.

Acknowledgment

This work was supported by the Korean Research Foundation Grant (KRF-2006-331-F00015) funded by the Korean Government (MOEHRD).

Appendix A. Supplementary material

CCDC 629017 and 629018 contain the supplementary crystallographic data for $Fe_3tdt_3(PEt_3)_3$ (**I**) and $Co_3tdt_3(PEt_3)_3$ (**II**), respectively. These data can be obtained free of charge via http://www.ccdc.cam.ac.uk/conts/retrieving.html, or from the Cambridge Crystallographic Data Centre, 12 Union Road, Cambridge CB2 1EZ, UK; fax: (+44) 1223-336-033; or e-mail: deposit@ccdc.cam.ac.uk. Supplementary data associated with this article can be found, in the online version, at doi:10.1016/j.poly.2007.01.052.

References

[1] Y.-U. Kim, J. Han, J. Kor. Soc. Appl. Biol. Chem. 48 (2005) 189.
[2] O. Einsle, F.A. Tezcan, S.L.A. Andrade, B. Schmid, M. Yoshida, J.B. Howard, D.C. Rees, Science 297 (2002) 1696.
[3] (a) U. Huniar, R. Ahlrichs, D. Coucouvanis, J. Am. Chem. Soc. 126 (2004) 2588;
(b) I. Dance, Chem. Commun. (2003) 324;
(c) T. Lovell, T. Liu, D.A. Case, L. Noodleman, J. Am. Chem. Soc. 125 (2003) 8377.
[4] T.-C. Yang, N.K. Maeser, M. Laryukhin, H.-I. Lee, D.R. Dean, L.C. Seefeldt, B.M. Hoffman, J. Am. Chem. Soc. 127 (2005) 12804.
[5] J. Han, D. Coucouvanis, J. Chem. Soc., Dalton Trans. (2005) 1234.
[6] J.W. Peters, W.N. Lanzilotta, B.J. Lemon, L.C. Seefeldt, Science 282 (1998) 1853.
[7] B.J. Lemon, J.W. Peters, Biochemistry 38 (1999) 12969.
[8] Y. Nicolet, C. Piras, P. Legrand, C.E. Hatchikian, J.C. Fontecilla-Camps, Structure 7 (1999) 13.
[9] D. Coucouvanis, J. Han, N. Moon, J. Am. Chem. Soc. 124 (2002) 216.
[10] J. Han, K. Beck, N. Ockwig, D. Coucouvanis, J. Am. Chem. Soc. 121 (1999) 10448.
[11] J. Han, M. Koutmos, S. Al Ahmad, D. Coucouvanis, Inorg. Chem. 40 (2001) 5985.
[12] F. Jiang, X. Xie, M. Hong, B. Kang, R. Cao, D. Wu, H. Liu, J. Chem. Soc., Dalton Trans. (1995) 1447.
[13] H.-R. Gao, T.C.W. Mak, B.-S. Kang, B.-M. Wu, Y.-J. Xu, Y.-X. Tong, X.-L. Yu, J. Chem. Res. S. (1996) 186.
[14] B. Kang, J. Peng, M. Hong, D. Wu, X. Chen, L. Weng, X. Lei, H. Liu, J. Chem. Soc., Dalton Trans. (1991) 2897.
[15] L.N. Mulay, E.A. Boudreaux (Eds.), Theory and Applications of Molecular Paramagnetism, Wiley-Interscience, New York, 1976.
[16] C. Goh, B.M. Segal, J. Huang, J.R. Long, R.H. Holm, J. Am. Chem. Soc. 118 (1996) 11844.
[17] S.C. Lee, R.H. Holm, Chem. Rev. 104 (2004) 1135.
[18] J. Han, D. Coucouvanis, J. Am. Chem. Soc. 123 (2001) 11304.
[19] J. Han, M. Huang, D. Coucouvanis, Polyhedron 21 (2002) 2523.
[20] M. Koutmos, H. Kalyvas, Y. Sanakis, A. Simopoulos, D. Coucouvanis, J. Am. Chem. Soc. 127 (2005) 3706.
[21] J. Chatt, L.A. Duncanson, L.M. Venanzi, J. Chem. Soc. (1955) 4461.
[22] D. Michael, P. Mingos, A.S. May, Structure and bonding aspects of metal cluster chemistry, in: D.F. Shriver, H.D. Kaesz, R.D. Adams (Eds.), Chemistry of Metal Cluster Complexes, VCH, New York, 1990, pp. 11–119 (Chapter 2).
[23] J.W. Lauher, J. Am. Chem. Soc. 100 (1978) 5305.
[24] D. Sellmann, M. Geck, F. Knoch, G. Ritter, J. Dengler, J. Am. Chem. Soc. 113 (1991) 3819.
[25] F.A. Cotton, Chem. Soc. Rev. 4 (1975) 27.
[26] A.R. Pinhas, R. Hoffmann, Inorg. Chem. 18 (1979) 654.
[27] K.B. Musgrave, H.C. Angove, B.K. Burgess, B. Hedman, K.O. Hodgson, J. Am. Chem. Soc. 120 (1998) 5325.
[28] V. Vrajmasu, E. Munck, E.L. Bominaar, Inorg. Chem. 42 (2003) 5974.
[29] W.P. Bosman, H.G.M. Van der Linden, J. Chem. Soc., Chem. Commun. (1977) 714.
[30] (a) V.K. Shah, W.J. Brill, Proc. Natl. Acad. Sci. USA 74 (1977) 3249;
(b) S.-S. Yang, W.-H. Pan, G.D. Friesen, B.K. Burgess, J.L. Corbin, E.I. Stiefel, W.E. Newton, J. Biol. Chem. 257 (1982) 8042.
[31] G. Philipp, H.A. Goodwin (Eds.), Spin Crossover in Transition Metal Compounds II, Springer, Berlin, Heidelberg, 2004.
[32] J. Vannimenous, G. Toulouse, J. Phys. C 10 (1977) L537.
[33] O. Kahn, Chem. Phys. Lett. 265 (1997) 109.
[34] O. Cador, D. Gatteschi, R. Sessoli, A.-L. Barra, G.A. Timco, R.E.P. Winpenny, J. Magn. Magn. Mater. 290–291 (2005) 55.
[35] L.J. Farrugia, J. Appl. Cryst. 30 (1997) 565.
[36] <http://www.expasy.org/spdbv/>.